Lecture 8:
Instabilities

E. J. Hinch

A large class of fluids flows is never observed in practice even though they are exact solutions to the equations of motion. This is because these flows are unstable to small perturbations that are always present in the environment. Newtonian fluid flows support a vast array of instabilities and it is not surprising that many of these instabilities persist when the Newtonian fluid is replaced by a non-Newtonian fluid. Additionally, there are a number of instabilities which are found only in non-Newtonian fluids.

In this lecture we survey six non-Newtonian flow instabilities. The first, the spinline draw resonance, is an instability of a simple viscous fluid that can be modified by non-Newtonian effects. Sections 2–4 deal with instabilities which depend on non-Newtonian effects for their existence. In section 5, we examine the little understood phenomenon of turbulent drag reduction in a dilute suspension of polymers. Finally, section 6 deals the instabilities of a high speed elastic jet.

1 Spinline Draw Resonance

The manufacture of synthetic fabrics such as nylon and kevlar involves the drawing of polymer melts into thin fibers on a spinline. The geometry of a simple spinline is shown in figure 1. As the draw ratio—the ratio of the velocity of the spindle to the exit velocity of the fluid—is increased, the spun fiber becomes thinner, so the spinning of extremely thin fibers requires large draw ratios. If the draw ratio is increased beyond a critical value,

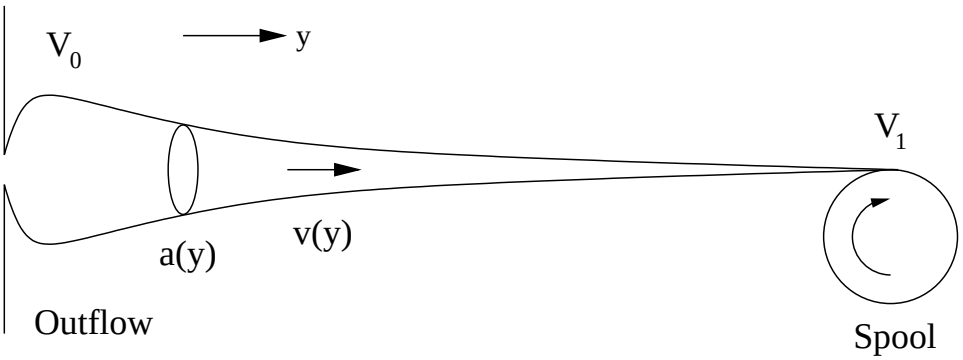

Figure 1: Geometry of a spinline.

the spinline draw resonance sets it. This instability, first described by Christensen [1] and Miller [2], is characterized by sustained periodic oscillations in the cross-sectional area and stress in the spinning polymer strand. While most fibers are spun from non-Newtonian fluids, the spinline draw resonance occurs even in purely Newtonian fluids. We will consider the simpler Newtonian instability first.

The geometry of a simple spinline is shown in figure 1. A steady state can be found by assuming that the cross-sectional area a and velocity v are functions of the streamwise coordinate y only. The continuity equation becomes a conservation equation for area,

$$\frac{\partial}{\partial y}(av) = 0, \tag{1}$$

while the momentum equation is a balance between the viscous force and the (constant) tension T:

$$\frac{T}{a} = \sigma_{yy} = 3\mu\frac{\partial v}{\partial y}. \tag{2}$$

The spinline has length L and boundary conditions

$$\begin{aligned} v(0) &= V_0 \\ v(L) &= V_1. \end{aligned} \tag{3}$$

The solution to equations (1)–(3) is

$$v(y) = V_0\,\mathrm{Dr}^{y/L} \tag{4}$$

$$a(y) = \frac{TL}{3\mu\ln\mathrm{Dr}}\,\mathrm{Dr}^{-y/L}, \tag{5}$$

where the $\mathrm{Dr} = V_1/V_0$ is the draw ratio.

This simple solution is unstable if

$$\mathrm{Dr} > 20.3.$$

Including additional processes can have a dramatic effect on this stability criterion. Inertia, cooling (which increases viscosity), and elastic effects can push the critical draw ratio to $\mathrm{Dr} \approx 10^3$. Surface tension and shear thinning, on the other hand, have a destabilizing influence and can lower the stability threshold to $\mathrm{Dr} \approx 3$. The exact stability threshold in an industrial application is set by a competition between these stabilizing and destabilizing effects.

To understand the mechanism for this instability, imagine a perturbation which causes a thinning of the thread near the spool (at $y = L$). Since the speed of the thread near the spool is fixed, the mass flux onto the spool must decrease, which decreases the total tension in the line. This low tension causes the velocity to decrease throughout the interior of the line. The speed of the thread at the outflow point (at $y = 0$) is similarly fixed, so the line must thicken near the outflow point to conserve mass (figure 2a). This thickened section will eventually propagate down the line to the spool. Once it reaches the spool, the increased mass flux onto the spool will increase the tension in the line, which causes the line to thin at the outflow point (figure 2b).

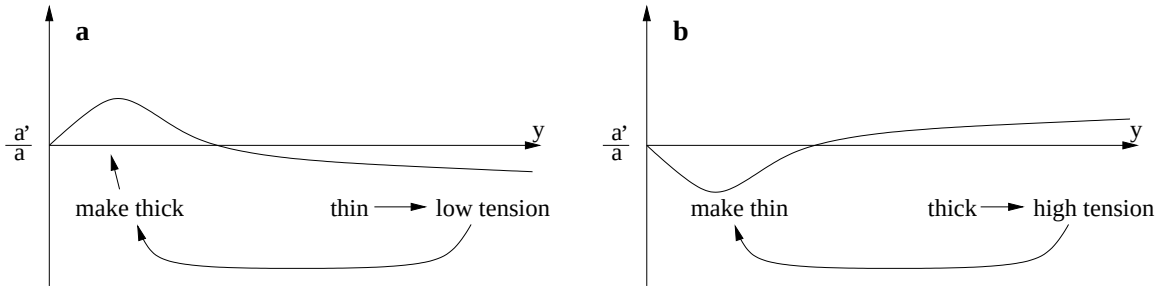

Figure 2: Mechanism for spinline draw resonance. (a) Thinning at the spool causes thickening at the outflow point. (b) Thickening at the spool causes thinning at the outflow point.

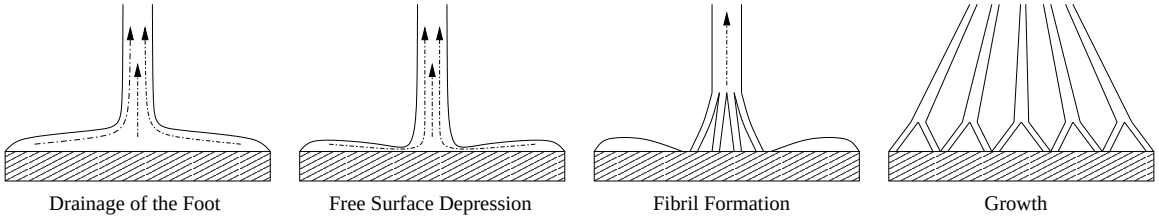

Figure 3: Development of the buckling instability, after Spiegelberg and McKinley's figure 10 [3]. The dash-dot curves represent streamlines.

The amplified feedback combined with the time delay caused by propagation feeds the instability. Above the critical draw ratio, the perturbation can grow to finite size. The system settles down into limit cycles, causing periodic oscillations in the thickness of the spun fiber.

2 Buckling Instability

The 'filament stretching device' is a common experimental device for measuring extensional properties of polymer solutions. In this device— which is described in detail in Lecture 2—a small cylinder of fluid is held between two rigid circular plates which are suddenly separated at a known rate. The extensional properties of the fluid are deduced by measuring the force on the plates as a function of the known strain. In order to obtain a consistent rheological measurement, the strain rate should be approximately constant throughout the extending fluid column. The buckling instability, which occurs on the plates of the filament stretching device, can seriously compromise the utility of the device unless measures are taken to prevent it. This instability was first observed by Spiegelberg and McKinley [3].

Figure 3 illustrates the evolution of the buckling instability. In the initial stages of the experiment, fluid is drained from the 'foot' of the column to feed the extending column. Eventually, the reservoir next to the column is depleted, at which time the foot begins to break up into fibrils. These fibrils migrate to the outer edge of the plate and can themselves develop secondary and tertiary instabilities.

The mechanism for this instability can be simply understood with the paradigm of

tension in curved streamlines. As the reservoir at the foot of the column is drained, the streamlines become increasingly more curved. Eventually, the tension in the streamlines is so great it overwhelms the adhesive force holding the column to the plate. This causes the center of the foot to detach from the plate, leaving the fibrils attached to the outer edge. The final configuration has nearly straight streamlines and thus forms a configuration which globally minimizes stored elastic energy. A mathematical investigation of the buckling instability can be found in Kumar and Graham [4].

Recent filament stretching devices have incorporated plates that contract as the filament is stretched. This modification stabilizes the foot of the column and allows consistent measurements of the extensional properties of the fluid [3].

3 Purely Elastic Instability of Curved Streamlines

A common feature of visco-elastic fluids is that instabilities can occur even in the absence of inertia. These are discussed at length in the review article [5]. Many of these occur in situations where the streamlines are curved. Streamlines in shear flow are under tension. If they are curved, this tension creates a *hoop stress*, which can lead to instabilities. The hoop stress acts in a direction opposite to the centrifugal effects, and so the resulting instabilities are clearly distinct from inertial effects.

The most famous example is the Taylor-Couette instability. In a Taylor-Couette device (two concentric rotating cylinders with fluid between them), an instability arises at sufficiently high flow rates. In a Newtonian fluid the instability occurs because of centrifugal effects at sufficiently high Taylor number (the Taylor number $4\frac{\Omega_1 R_1^2 - \Omega_2 R_2^2}{R_2^2 - R_1^2}\frac{\Omega_1 d^4}{\mu^2}$ is the ratio of centrifugal force to viscous force), but in a non-Newtonian fluid an instability can occur at negligible Taylor number (e.g., 10^{-8}). The mechanism creating the instability is the hoop stress generated by the flow which acts oppositely to the expected centrifugal force. This instability was first observed and analyzed by [6, 7, 8]. Further experimental analysis was done by [9] and by a number of other people. For a gap ratio of $\epsilon \equiv (R_2 - R_1)/R_2$, the instability appears to happen when $\epsilon^{1/2}\mathrm{Wi} \approx 8$ (note that $\epsilon^{1/2}\mathrm{Wi} = \sqrt{\mathrm{DeWi}}$).

Numerics suggest that axisymmetric and non-axisymmetric modes can occur, and both are observed in experiments. The instability occurs as a supercritical Hopf bifurcation.

Other flows with curved streamlines can be found in Taylor-Dean, plate-plate or cone and plate geometries. This general class of instabilities has led to the concept of *elastic turbulence* [10], a complicated time-dependent flow with negligible Reynolds number.

4 Instability of coextrusion

Even in flow with straight streamlines instabilities can occur in inertialess flow with elasticity. In core-annular flow of two fluids down a pipe, differences in elastic properties can lead to instability at zero Reynolds number. We consider a pipe with flow in the $\hat{\boldsymbol{z}}$ direction, with one fluid at $r < r_0$ and another at $r_0 < r < R$. At the interface between the two fluids $\sigma \cdot \boldsymbol{n}$ must be continuous. If the elastic properties of the two fluids are different, there will be a discontinuity of the σ_{zz} component because the two fluids have different first normal

stress differences. However, since $\boldsymbol{n}$ has no component in the $\hat{\boldsymbol{z}}$ component, $\sigma \cdot \boldsymbol{n}$ remains continuous.

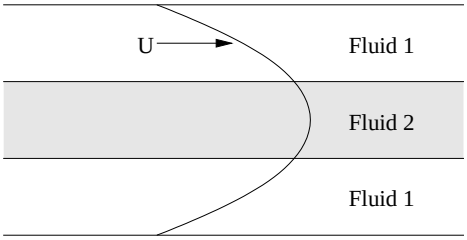

(a) The unperturbed basic flow.

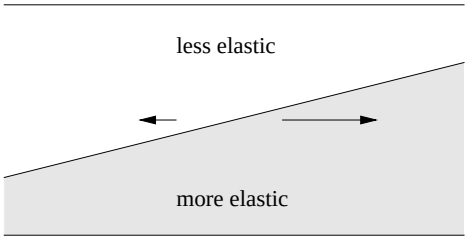

(b) Zooming in on a perturbed interface. Because the fluids have different elasticities, the interface moves to the right.

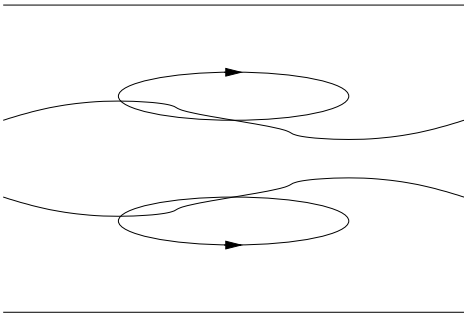

(c) A small core which is more elastic than the outer fluid. Since the core is small, the recirculation occurs in the outer fluid and enhances the perturbation to the interface

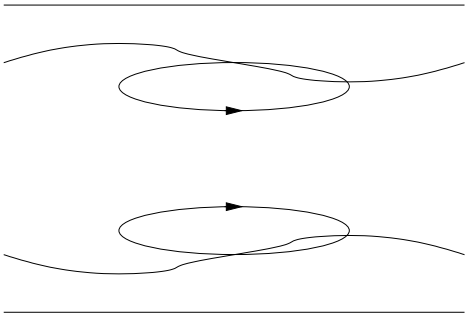

(d) A perturbation with a large core which is more elastic than the outer fluid. Here the recirculation occurs in the core and opposes the perturbation to the interface.

Figure 4: Mechanism of instability: The misalignment of the interface and the base flow creates a perturbation flow. Incompressibility forces the flow to recirculate. The recirculation can either enhance or oppose the perturbation to the interface.

When there is a perturbation to the interface, $\boldsymbol{n}$ is no longer purely radial, so a secondary flow across the interface must develop to keep $\sigma \cdot \boldsymbol{n}$ continous. Physically the more elastic fluid is pulling the less elastic fluid across the curved interface. The secondary flow must have a recirculation by conservation of mass. If the inner fluid takes up a large fraction of the pipe, the recirculation will take place inside the inner fluid. If it takes up a small fraction of the pipe, the recirculation will take place inside the outer fluid. Thus the recirculation will either enhance or stabilize the perturbation, depending on which fluid is more elastic.

This instability was first computed in the longwave limit by [11], and the mechanism was explained by [12]. It was found that if the more elastic fluid occupied less than 32% of the volume the flow would be unstable to long waves, regardless of whether the more elastic fluid was in the core or the annulus.

This instability has been studied in detail in her PhD thesis by Wilson [13]. It was further found that when the discontinuity is smoothed out, the instability can be eliminated [14].

5 Turbulent Drag Reduction

It was noted during the second world war that the addition of a small amount of high molecular weight polymers to gasoline dramatically reduced the effective turbulent viscosity of the flow. Since then it has been shown that drag reduction of a turbulent flow is a general feature of dilute solutions of long polymers. Though it is potentially of extreme industrial value, a detailed explanation of this phenomenon remains elusive. However, a general framework for understanding this effect has emerged.

The action of the polymers is primarily to modify turbulent behavior near the walls. There, wall eddies are formed which transport momentum into the fluid interior which exerts a drag on the flow. The polymer's high resistance to extension makes these eddies wider and less frequent and, consequently, less efficient in transporting momentum away from the walls. Cross-stream fluctuations are suppressed relative to their Newtonian values while alongstream fluctuations are actually enhanced. The traditional explanation for turbulent drag reduction—that the addition of polymers reduces the turbulent intensity of the flow—cannot hold since the turbulent intensity in the bulk of the fluid is unaffected by the presence of polymers. (This explanation follows that in [15].) Figure 5 shows numerical simulations of the effect of polymers on the mean flow and near-wall velocity fluctuations.

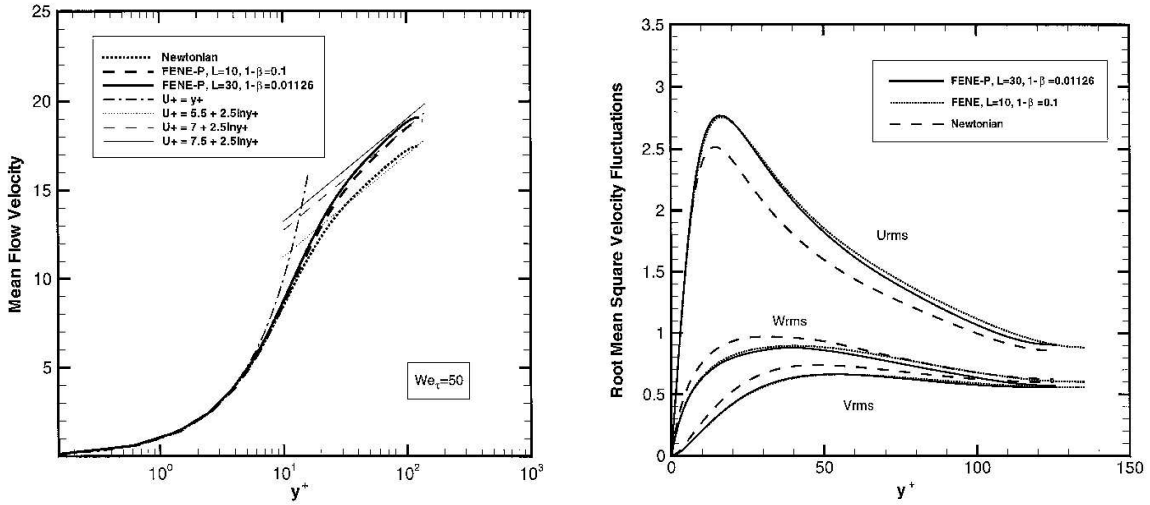

Figure 5: Numerical simulations of turbulence using Newtonian and two different FENE rheologies, from [15]. Left: Mean flow velocity in the log-layer near the wall. Right: RMS velocity fluctuations near the wall. The wall coordinate $y^+ \equiv \nu y/\nu_0$ where ν_0 is the viscosity of fluid and ν is the effictive viscosity.

6 Instability of a High Speed Elastic Jet

We now look at an instability which happens at high Reynolds number and high Weissenberg number. We consider a high speed submerged elastic jet [16, 17]. It is well known that a high extensional viscosity helps prevent an elastic jet from breaking up into spray, so elasticity helps stabilize that instability. However, other instabilities can arise. We follow [17] to consider the effect of elasticity using an Oldroyd-B model.

6.1 Governing Equations

The equations of motion are

$$\begin{aligned}\nabla \cdot \boldsymbol{U} &= 0\\ \rho\frac{D\boldsymbol{U}}{Dt} &= -\nabla P + \mu\nabla^2\boldsymbol{U} + G\nabla\cdot\mathsf{A}\\ \overset{\triangledown}{A} &= -\frac{1}{\tau}(\mathsf{A}-\mathsf{I})\end{aligned}$$

The basic state has flow in only the x direction. It is steady and rectilinear, so $\frac{D\mathsf{A}}{Dt}=0$. We get

$$\begin{aligned}\boldsymbol{U} &= (U(y,z),0,0)\\ \mathsf{A} &= \begin{bmatrix}1+2\tau^2(U_y^2+U_z^2) & \tau U_y & \tau U_z\\ \tau U_y & 1 & 0\\ \tau U_z & 0 & 1\end{bmatrix}.\end{aligned}$$

We now make the assumption that the Reynolds number is large, $\frac{\rho UL}{\mu+G\tau}\gg 1$, and that the Weissenberg number is large as well, $\frac{U\tau}{L}\gg 1$.

6.2 Linearization

The problem is linearized with lower case letters denoting the perturbation quantities. We denote the components of the perturbed velocity by $\boldsymbol{u}=(u,v,w)$. The linearized equations are

$$\begin{aligned}u_x+v_y+w_z &= 0\\ \rho[u_t+Uu_x+vU_y+wU_z] &= -p_x+G[a_{11,x}+a_{12,x}+a_{13,z}]\\ \rho[v_t+Uv_x] &= -p_y+Ga_{12,x}\\ \rho[w_t+Uw_x] &= -p_z+Ga_{13,x}\\ a_{11,t}+Ua_{11,x}+vA_{11,y}+wA_{11,t} &= 2A_{11}u_x+2a_{12}U_y+2a_{13}U_z\\ a_{12,t}+Ua_{12,x} &= A_{11}v_x\\ a_{13,t}+Ua_{13,x} &= A_{11}w_x\end{aligned}$$

and we seek a solution proportional to $e^{i\alpha(x-ct)}$ where the wavenumber α is real and the growth rate is αc.

We can make progress using different coordinates. We change to streamline displacements. We let η denote the y-displacement of a material particle from its equilibrium position and ζ denote its z-displacement. Then $\frac{D\eta}{Dt} = v$ to first order, but we can express $\frac{D\eta}{Dt}$ to first order as

$$\begin{aligned}\frac{D\eta}{Dt} &= \eta_t + (U\cdot\nabla)\eta \\ &= \eta_t + (U\frac{\partial}{\partial x})\eta \\ &= i\alpha(U-c)\eta\end{aligned}$$

so $v = i\alpha(U-c)\eta$. A similar analysis can be done for ζ. By incompressibility

$$u = -\eta U_y - \zeta U_z - (U-c)(\eta_y + \zeta_z)$$

and

$$\begin{aligned}a_{12} &= i\alpha\eta A_{11} \\ a_{13} &= i\alpha\zeta A_{11} \\ a_{11} &= -2A_{11}(\eta_y+\zeta_z) - (\eta A_{11,y} + \zeta A_{11,z}).\end{aligned}$$

We use these to arrive at

$$\begin{aligned}i\alpha[\rho(U-c)^2 - GA_{11}](\eta_y+\zeta_z) &= i\alpha p \\ [\rho(U-c)^2 - GA_{11}]\alpha^2\eta &= p_y \\ [\rho(U-c)^2 - GA_{11}]\alpha^2\zeta &= p_z.\end{aligned}$$

In planar flow we set $\zeta = 0$ and $\eta = -\phi/(U-c)$ to arrive at an elastic Rayleigh equation

$$\frac{d}{dy}\left([\rho(U-c)^2 - GA_{11}]\frac{d}{dy}\frac{\phi}{U-c}\right) = \alpha^2[\rho(U-c)^2 - GA_{11}]\frac{\phi}{U-c}.$$

This can be expressed in a self-adjoint form, giving a semi-circle theorem [18] which states that the complex wave speed c must lie within a circle centered on $(U_{\max}+U_{\min})/2$ with radius $(U_{\max}-U_{\min})/2$.

We assume that the time-scale of the instability is much less than vorticity diffusion, stress relaxation and shear wave propogation.

6.3 Two-dimensional jet

We consider a two dimensional jet where

$$U(y) = \begin{cases} U_0\left(1-\frac{y^2}{b^2}\right) & |y|\le b \\ 0 & |y|>b\end{cases}$$

$$GA_{11} = \begin{cases} \frac{8G\tau^2U_0^2y^2}{b^4} & |y|\le b \\ 0 & |y|>b\end{cases}$$

We define the elasticity number

$$E = \frac{GA_{11}}{\rho U^2} = \frac{G\tau^2}{\rho b^2}$$

which, remarkably, is independent of the flow rate. Outside the jet we have a potential flow

$$p = e^{\mp\alpha y}$$
$$\eta = \mp\frac{e^{\mp\alpha y}}{\alpha c^2}$$

We look for sinuous and varicose modes to see the effect of the elasticity parameter E on the growth rates.

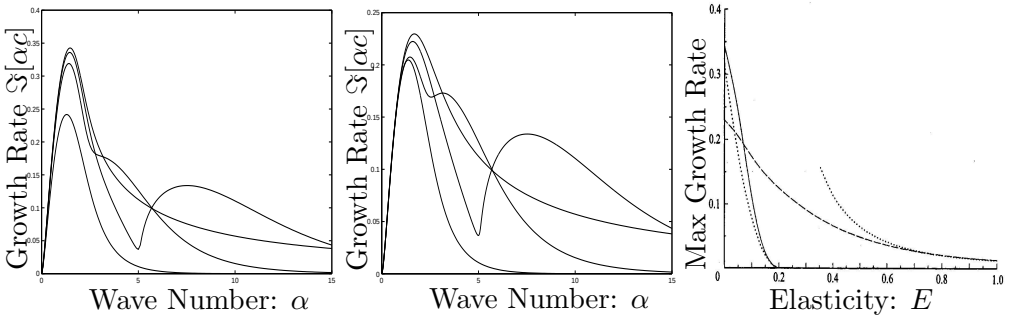

(a) The growth rate of the instability as a function of k for sinuous disturbances with E equaling 0, 0.0025, 0.01 and 0.05. The highest peak occurs for $E = 0$, and the peak decreases as E increases.

(b) The growth rate of the instability as a function of k for varicose disturbances with E equaling 0, 0.0025, 0.01 and 0.05. The highest peak occurs for $E = 0$, and the peak decreases as E increases.

(c) The maximum growth rate of the 2D jet as a function of the elsaticity for the sinuous mode (continuous curve) and the varicose mode (dashed curve). The dotted curves are asymptotic results for long waves.

Figure 6: Growth rates — Elasticity stabilizes both instabilities. For small (nonzero) E, there appears to be an elastic wave mode at large wavenumber.

As the elasticity approaches 0, there is an unstable mode with moderate growth rate at large α. As E decreases further, the value of α increases. This instability is localized close to the interface, and depends on the discontinuity in shear rates. As the discontinuity in shear rates leads to a jump in normal stresses, this may be similar to the coextrusion instability in origin.

6.4 Conclusions

The elasticity has a stabilizing effect. For a two-dimensional jet, the sinuous mode is no longer unstable when $E \geq 0.2$. The varicose mode remains unstable as E increases, but the maximum growth rate decays to 0.

For an axisymmetric jet, it was shown by Batchelor and Gill [19] that the Newtonian case is stable to varicose perturbations. Adding a small amount of elasticity allows the emergence of an unstable mode for large α. However, as the elasticity increases, this unstable mode is damped and stabilized at $E = 0.228$. The sinuous mode is stabilized at $E = 0.3756$.

Notes by Joel C. Miller and Christopher L. Wolfe

References

[1] R. E. Christensen, "Extrusion coating of polypropylene," Soc. of Pet. Engineers J. **18**, 751 (1962).

[2] J. C. Miller, "Swelling behaviour in extrusion," Soc. of Pet. Engineers Trans. **3**, 134 (1963).

[3] S. Spiegelberg and G. McKinley, "Stress relaxation and elastic decohesion of viscoelastic polymer solutions in extensional flow," J. Non-Newt. Fluid Mech. **67**, 49 (1996).

[4] K. Kumar and M. Graham, "Buckling instabilities in models of viscoelastic free surface flows," J. Non-Newt. Fluid Mech. **89**, 337 (2000).

[5] E. S. G. Shaqfeh, "Purely elastic instabilities in viscometric flows," Annual Review of Fluid Mechanics **31**, 129 (1996).

[6] S. J. Muller, R. G. Larson, and E. S. G. Shaqfeh, "A purely elastic transition in taylor-couette flow," Rheologica Acta **28**, 499 (1989).

[7] R. G. Larson, E. S. G. Shaqfeh, and S. J. Muller, "The effect of fluid rheology on the elastic taylor-couette instability," Journal of Non-Newtonian Fluid Mechanics **51**, 195 (1994).

[8] E. S. G. Shaqfeh, S. J. Muller, and R. G. Larson, "The effects of gap width and dilute solutions properties on the viscoelastic instability," Journal of Fluid Mechanics **235**, 285 (1992).

[9] A. Groisman and V. Steinberg, "Mechanism of elastic instability in taylor-couette flow in polymer solutions: experiment," Physics of Fluids **10**, 2451 (1998).

[10] A. Groisman and V. Steinberg, "Elastic turbulence in a polymer solution flow," Nature **405**, 53 (2000).

[11] K. P. Chen, "Interfacial instability due to elastic stratification in concentric coextrusion of two viscoelastic fluids," Journal of Non-Newtonian Fluid Mechanics **40**, 155 (1991).

[12] E. J. Hinch, O. J. Harris, and J. M. Rallison, "The instability mechanism for two elastic liquids being co-extruded," Journal of Non-Newtonian Fluid Mechanics **43**, 311 (1992).

[13] H. J. Wilson, Ph.D. thesis, Cambridge University, Cambridge, United Kingdom, 1998.

[14] H. J. Wilson and J. M. Rallison, "Instability of channel flow of a shear-thinning white metzner fluid," Journal of Non-Newtonian Fluid Mechanics **87**, 75 (1999).

[15] C. D. Dimitropoulos, R. Sureshhumar, and A. N. Beris, "Direct numerical simulation of viscoelastic turbulent channel flow exhibiting drag reduction: effect of the variation of rheological parameters," J. Non-Newt. Fluid Mech. **79**, 433 (1998).

[16] J. Azaiez and G. M. Homsy, "Linear stability of free shear flow of viscoelastic liquiids," Journal of Fluid Mechanics **268**, 37 (1994).

[17] J. M. Rallison and E. J. Hinch, "Instability of a high-speed submerged elastic jet," Journal of Fluid Mechanics **288**, 311 (1995).

[18] L. N. Howard, "Note on a paper by J. W. Miles," Journal of Fluid Mechanics **10**, 509 (1961).

[19] G. K. Batchelor and A. E. Gill, "Analysis of the stability of axisymmetric jets," Journal of Fluid Mechanics **14**, 529 (1962).